IEEE Access
Multidisciplinary ⋮ Rapid Review ⋮ Open Access Journal

Received 9 April 2023, accepted 28 April 2023, date of publication 9 May 2023, date of current version 17 May 2023.

Digital Object Identifier 10.1109/ACCESS.2023.3274605

RESEARCH ARTICLE

Optimal Multiple FSO Transceiver Configuration for Using on High-Altitude Platforms

DIEU LINH TRUONG[1] AND THE NGOC DANG[2], (Member, IEEE)
[1]School of Information and Communication Technology, Hanoi University of Science and Technology, Hanoi 100000, Vietnam
[2]Department of Wireless Communications, Posts and Telecommunication Institute of Technology, Hanoi 100000, Vietnam

Corresponding author: Dieu Linh Truong (linhtd@soict.hust.edu.vn)

ABSTRACT Free-space optical (FSO) communication requires light of sight (LoS) between the transmitter and the receiver. For long-distance communication, many research projects have been conducted towards using a network composed of high-altitude platforms (HAPs) flying at an elevation of 20 km to carry intermediate FSO transceivers that forward data between ground stations. The clear environment at high elevations prevents terrestrial obstacles from cutting the LoS between the transceivers. An FSO transceiver on a HAP can communicate with ground stations within a small area owing to its limited beam size. We suggest using multiple FSO transceivers on a HAP to extend its ground coverage. However, the use of too many FSO transceivers may quickly exhaust the onboard energy of the HAP. As a result, HAP must be lowered to recharge frequently. In this study, we first propose a configuration of multiple FSO transceivers to widen the ground coverage of a HAP. We then propose a set of closed-form expressions to calculate the extended coverage. Finally, to implement a HAP network using multiple FSO transceivers, we seek the optimal configuration of multiple FSO transceivers that minimizes the total cost of the HAP network, including amortization, energy, and maintenance costs. The simulation results show that the proposed multiple FSO transceiver configuration can increase four times the ground coverage area of a HAP and significantly reduces the cost of the HAP network.

INDEX TERMS Free space optics, high-altitude platform, beam size optimization, HAP based FSO network.

I. INTRODUCTION

Free-space optical (FSO) communication uses light propagation in free space to transmit data. In recent years, this technology has emerged as a promising choice for short-distance high-speed communication between endpoints with a clear light of sight (LoS). Commercial FSO transmitters available in the market at prices of thousands of dollars can operate at $1.25-10$ Gbps over $1-2$ kilometers, for example, the SONABeam series of fSona [1].

To reach a long distance, a multi-hop FSO system can be used, where data are transmitted through intermediate FSO transceivers [2], [3]. To avoid obstacles that cut the LoS between terrestrial FSO transceivers, researchers from academia and industry have proposed placing intermediate FSO transceivers of the multi-hop FSO system on high-altitude platforms (HAPs). High-altitude platforms are flying objects that operate at altitudes of 17-24 km in the stratosphere. Researches on HAPs have been reported since 1990s with numerous perspective applications including deploying 2G/3G coverage; extending communication over rural areas, providing broadband radio communication services using millimeter wavelengths, remote sensing, restoring a failure communication after a disaster thanks to quick deployment; and military communications [4]. Several HAP models have been proposed and piloted under previously ended projects such as HALO, STRATOS, HeliNet, CAPANINA, HAPCOS, SkyNet [5] or still continuing Stratobus project of Thales Alenia Space [6]. Most of researches focused on using radio frequency for the communications between HAP and the ground leading to limited data rate. Recent research projects, for example, the Loon Project of Google [7], the Aquila program of Facebook [8] stated the focus on FSO communications between HAP and the ground resulting in much higher data rate.

The associate editor coordinating the review of this manuscript and approving it for publication was Zhenzhou Tang.

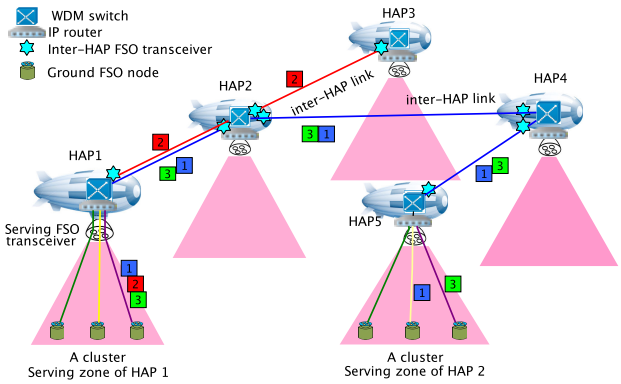

FIGURE 1. Multi-hop FSO communication system using HAP [9].

A multi-hop FSO system using a HAP network is described in [9] and illustrated in Figure 1. According to this model, FSO transceivers on the ground (so-called ground FSO nodes) are regrouped into clusters to become the serving zones of HAPs. A HAP has an FSO transceiver looking down to exchange data with the ground FSO nodes of the cluster under it. This FSO transceiver is called *serving* FSO transceiver. A HAP also carries several FSO transceivers pointing towards other HAPs for inter-HAP communication. These FSO transceivers are known as *inter-HAP* FSO transceivers.

An end-to-end data-switching scheme for a multi-hop FSO system using HAPs was proposed in [9]. Since the communication between a HAP and the ground is point-to-multipoint, the *serving* FSO transceiver on the HAP controls multiple accesses from ground FSO nodes under it using the wavelength devision multiplexing (WDM) technique. Each ground node is assigned a separate wavelength for up and down communication. An IP router on the HAP aggregates IP packets heading toward a common cluster within a single flow. The flow will be carried by one or more continuous lightpaths between the source and destination HAPs. The number of lightpaths is determined according to the size of the flow and the transport capacity of a wavelength. A WDM switch is installed on each HAP to route these lightpaths over the HAP network on a wavelength-switched basis. In Figure 1, the blue path HAP1-HAP2-HAP4-HAP5 and the red path HAP1-HAP2-HAP3 are two flows.

Although the International Telecommunication Union (ITU) recommends a HAP footprint width of approximately 500 km in radius, experimental projects show much smaller coverage areas [10]. Nevertheless, a network of multiple HAPs can cover a country entirely. For example, a constellation of 16 HAPs with multiple radio frequency antennas was considered to cover Japan [11].

In terrestrial FSO communications, the light beams are usually set to be very narrow for low transmission energy. However, for HAP and ground communication, the *serving* FSO transceiver of the HAP must project a sufficiently wide laser beam to obtain a large footprint. Research in [12] shows that the laser source from HAP should be very powerful for providing such a large ground coverage.

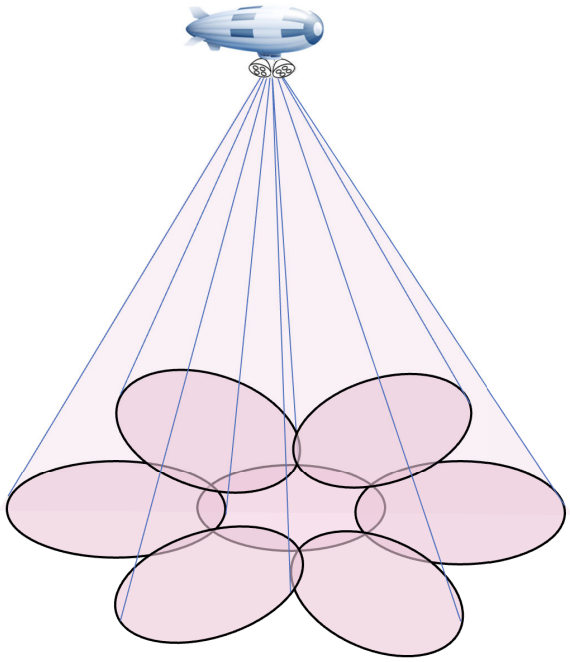

FIGURE 2. A HAP with multiple *serving* FSO transceivers and its footprint.

A single *serving* FSO transceiver provides a relatively small footprint owing to the low capacity of the current laser source, and the limited sensibility and aperture sizes of ground receivers. The calculations in Section II-A shows that with a laser source of 1 W, required received power of -49.62 dBm, and receiver telescope aperture radius of 0.75 m, a single *serving* FSO transceiver at an elevation of 20 km can cover a ground area of 6.691 km radius only (see Table 3).

To extend the coverage of a HAP, we propose using multiple *serving* FSO transceivers arranged in a bundle, as shown in Figure 2. Each *serving* FSO transceiver points in a slightly different direction to cover a particular ground area that overlaps other areas to create a continuous coverage region. Given a ground region to be served, using HAPs with multiple *serving* FSO transceivers reduces the number of required HAPs compared to using HAPs with a single *serving* FSO transceiver. However, the expenditure for *serving* FSO transceivers increases. Therefore, the number of *serving* FSO transceivers to be used on a HAP should be carefully considered.

In this study, we focus on identifying the optimal configuration of multiple *serving* FSO transceivers to achieve a minimal-cost HAP network for serving a set of ground FSO nodes. The optimal configuration should define the number of *serving* FSO transceivers to be set up on a HAP and the beam width for each transceiver. The cost of the HAP network includes the investment, energy, and maintenance costs.

Regarding the communication between ground nodes and a HAP, the multiple *serving* FSO transceiver model still uses the WDM technique, where each ground node is assigned a unique wavelength within its cluster to communicate with its HAP. The number of ground nodes to be served by a HAP is restricted by the number of wavelengths offered by the WDM technique.

Compared with the previous studies in [9] and [12], the current research differs in two aspects. First, the current research proposes to use multiple *serving* FSO transceivers on each HAP instead of a single *serving* FSO transceiver, as in [9] and [12]. Second, the current research identifies the optimal beam widths for *serving* FSO transceivers, whereas in [9], the beam widths are predefined.

The current study also differs from that in [13], where beam size was optimized for an inter-HAP link, which is a point-to-point link.

The remainder of this paper is organized as follows. First, we analyze the single and multiple *serving* FSO transceivers configurations in Section II to determine their ground coverage sizes and constraints on transmitter beams. In Section III, we state the problem of designing a minimal-cost HAP-based FSO network, which is the target of the optimization of multiple *serving* FSO transceiver configuration. Then, in Section IV, we define a HAP energy consumption formula and show that solar energy is necessary for keeping the HAP working in space for a long period. We also present a constraint that a HAP must respect to relying uniquely on solar energy. In Section V, we present the algorithms for identifying the optimal multiple *serving* FSO transceiver configuration and its footprint radius. Section VI presents the process designing the minimal cost HAP-based FSO network using the optimal multiple *serving* FSO transceiver configuration. Section VII presents the simulation results. Finally, Section VIII concludes the paper.

II. SERVING FSO TRANSCEIVER CONFIGURATIONS

A. SINGLE SERVING FSO TRANSCEIVER CONFIGURATION

In this section, the allowable beam width and ground coverage of a single *serving* FSO transceiver are determined. The beam size is restricted to ensure that the received power at a ground point within the beam footprint is detectable by receivers.

Assume that the transmitter source radiates within a solid angle α and that the radiation density is uniform in all directions within the solid angle at a distance r from the source. The radiation density at distance r is inversely proportional to the surface of the part of the sphere radius r blocked by the solid angle α. To calculate this surface, we divide the sphere into thin ribbons corresponding to open angles of $d(\alpha/2)$. The width of a ribbon is $rd(\alpha/2)$, as shown in Figure 3. The radius of the ribbon at zenith angle $\alpha/2$ is $r\sin(\alpha/2)$. Thus, the ribbon surface is $2\pi r\sin(\alpha/2)rd(\alpha/2)$. The surface of the part of the sphere blocked by the solid angle α is the sum of the surfaces of all ribbons when zenith angle varies from α to 0, as follows:

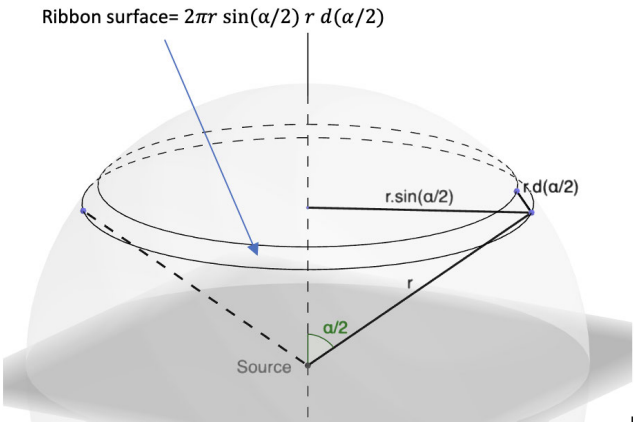

FIGURE 3. Surface of the part of sphere blocked by solid angle α is calculated as the sum of the surface of all ribbons around the sphere when the solid angle varies from α to 0.

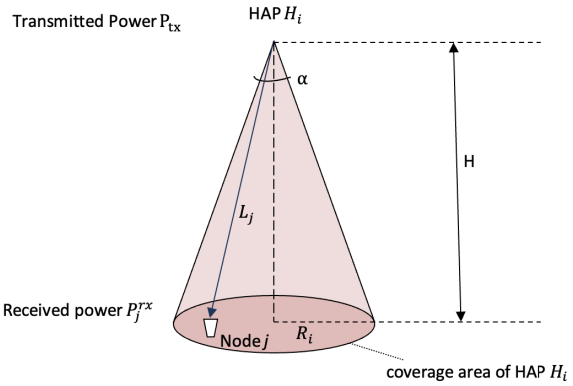

FIGURE 4. Received power on border nodes of a coverage area is the smallest amongst all nodes in the area.

$$\int_{\alpha}^{0} 2\pi r\sin(\frac{\alpha}{2})rd(\frac{\alpha}{2}) = 2\pi r^2(1-\cos(\frac{\alpha}{2}))$$

Let U_r be the radiation density at distance r and P_{tx} be the transmitted power at the source. We deduce:

$$U_r = \frac{P_{tx}}{2\pi r^2(1-\cos(\alpha/2))} \quad (1)$$

Let P_j^{rx} be the received power at ground FSO node j. Assume that each ground node uses a telescope at its receiver to capture more signal power from its HAP. The received power is proportional to the radiation density and the receiver telescope aperture of the ground node. It is:

$$P_j^{rx} = e^{-\sigma L_j}U_{L_j}A_R \quad (2)$$

where

- L_j is the distance between ground FSO node j and its *serving* HAP H_i (see Figure 4),
- σ is the attenuation coefficient of the links between the HAP and ground,

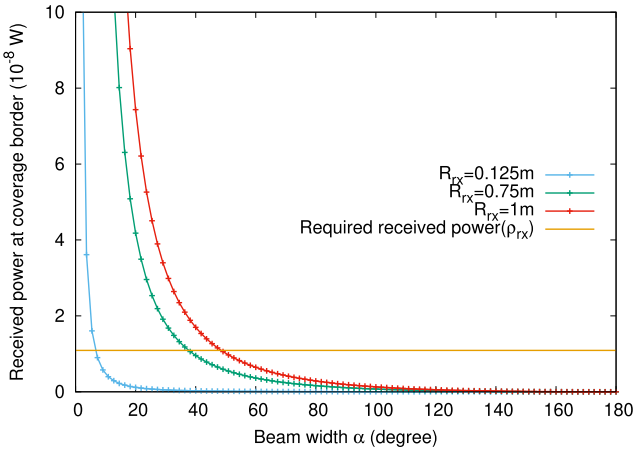

FIGURE 5. Received power at the coverage border of the single *serving* FSO transceiver configuration with different receiver telescope apertures when $P_{tx} = 1$ W, $\rho_{\text{rx}} = -49.62$ dBm.

- U_{L_j} is radiation density at distance L_j from the source,
- A_R is the receiver telescope aperture area of a ground FSO node. Let $\mathbb{R}_{\text{rx}}$ be the receiver telescope aperture radius, then, $A_R = \pi \mathbb{R}_{\text{rx}}^2$.

In (2), the first term represents the attenuation of laser power through the atmosphere, which is described by the exponential Beer-Lambert Law [14].

By substituting U_{L_j} from (1) into (2), we obtain the received power at node j as follows:

$$P_j^{rx} = e^{-\sigma L_j} \frac{P_{tx} \mathbb{R}_{\text{rx}}^2}{2L_j^2(1 - \cos(\alpha/2))} \tag{3}$$

The power received at node j must not be less than the required level of the receiver, denoted by ρ_{rx}. It is obvious that node j at the border of the ground coverage area receives the least power because it is the furthest from the source (see Figure 4). Hence, all nodes in the coverage areas of HAP H_i receive sufficient power if and only if the border nodes receive at least the required power; that is,

$$\boxed{P_j^{rx} = e^{-\sigma \mathbb{H}/\cos(\frac{\alpha}{2})} \frac{P_{tx} \mathbb{R}_{\text{rx}}^2 \cos^2(\frac{\alpha}{2})}{2\mathbb{H}^2(1 - \cos(\frac{\alpha}{2}))} \geq \rho_{\text{rx}}} \tag{4}$$

where L_j is substituted by $\mathbb{H}/\cos(\frac{\alpha}{2})$ for border node j.

Solving inequation (4) yields the beam width of the single *serving* FSO transceiver configuration. Corresponding to beam width α, the ground coverage radius of the configuration is:

$$R_i = \mathbb{H} \tan\left(\frac{\alpha}{2}\right) \tag{5}$$

Lemma 1: Function P_j^{rx} decreases with $\alpha \in [0..\pi]$.
Proof of Lemma 1 is given in Appendix A.

Figure 5 shows the received power at a border node of the coverage area with different receiver telescope aperture radius $\mathbb{R}_{\text{rx}}$. The transmitted power is set to $P_{tx} = 1$ W and $\rho_{\text{rx}} = -49.62$ dBm (equivalent to 1.09×10^{-8}W). This figure confirms that P_j^{rx} decreases with an increase in α.

Let α_{max} be the value for α that makes $P_j^{rx}(\alpha_{max}) = \rho_{\text{rx}}$; then according to Lemma 1,

$$P_j^{rx}(\alpha) \geq P_j^{rx}(\alpha_{max}) = \rho_{\text{rx}}, \forall \alpha \in [0..\alpha_{max}]$$

That means all $\alpha \in [0..\alpha_{max}]$ satisfy constraint (4).

Calculations using the parameters given in Table 1 show that when $\mathbb{R}_{\text{rx}} = 0.75$ m, the size of the telescope built by NICT Japan in 1988 [15], α_{max} reaches 37° and the coverage radius is 6691 m. When $\mathbb{R}_{\text{rx}} = 1$ m, $\alpha_{max} = 49°$ and the coverage radius is 9114 m.

B. MULTIPLE SERVING FSO TRANSCEIVER CONFIGURATION

The ground coverage of a HAP can be widened by combining several *serving* FSO transceivers. Different combinations are possible. In this research, we study a straightforward configuration in which a principal *serving* FSO transceiver is in the center projecting light perpendicular to the ground, and several identical supplementary *serving* FSO transceivers are set evenly around the principal one (Figure 6). Each supplementary transceiver projects slanted beams to extend the coverage in one direction. In this study, this arrangement is referred to as *m*FSO configuration. Usually, the transmitters in a bundle are considered to project signals in parallel. However, because of the large principal beam, the supplementary *serving* FSO transceiver projection directions are far from being perpendicular to the ground, and their footprints must be considered as ellipses instead of circles.

To create a continuous coverage region, the footprint of the principal *serving* FSO transceiver and those of the supplementary *serving* FSO transceivers should overlap. Therefore, there should be a sufficiently large number of supplementary *serving* FSO transceivers to cover entirely the contour of the principal footprint. The extended coverage area is defined as the largest circle covered by these footprints (Figure 6). The principal transceiver is responsible for the region defined by its footprint. A supplementary *serving* FSO transceiver is responsible for the part limited by its footprint, principal coverage circle, and extended coverage circle.

Let α be always the beam width of the principal *serving* FSO transceiver. To ensure that ground nodes under principal coverage receive sufficient power, α should still respect constraint (4), as in the single *serving* FSO transceiver configuration.

Let the beam width of a supplementary *serving* FSO transceiver be β. In the responsible area of the supplementary transceiver, the points on the extended coverage circle are the farthest from the supplementary transceiver; thus, they receive the least power. If these points receive at least ρ_{rx}, all other points receive sufficient power.

It is easy to note that the footprints of the neighboring supplementary *serving* FSO transceivers join each other on the extended coverage circle. Let J be such a joint point, the power J receives from the supplementary FSO transceiver is

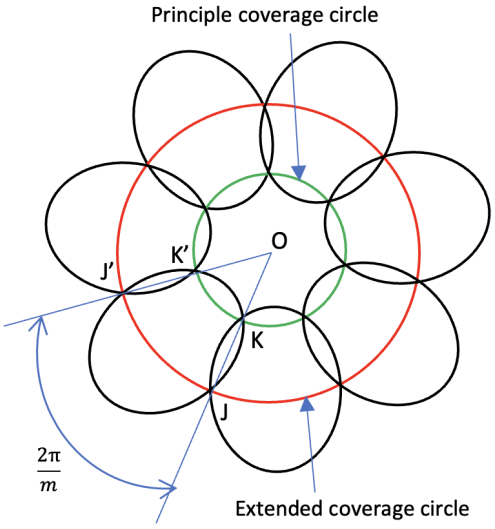

FIGURE 6. Footprint of a multiple FSO transceiver (*m*FSO) configuration with *m* supplementary *serving* FSO transceivers.

defined similar to (3) but with beam width β, which is

$$P_J^{rx} = e^{-\sigma \times L_J} \frac{P_{tx}\mathbb{R}_{\text{rx}}^2}{2L_J^2(1-\cos(\beta/2))} \tag{6}$$

Thus, β is constrained by the condition $P_J^{rx} \geq \rho_{\text{rx}}$, which gives:

$$\boxed{e^{-\sigma \times L_J} \frac{P_{tx}\mathbb{R}_{\text{rx}}^2}{2L_J^2(1-\cos(\beta/2))} \geq \rho_{\text{rx}}} \tag{7}$$

Let us denote the extended coverage radius by R_{ext} then

$$\boxed{L_J = \sqrt{\mathbb{H}^2 + R_{\text{ext}}^2}} \tag{8}$$

Appendix B presents detailed calculations of L_J and R_{ext}. The calculations yielded the following results

$$\boxed{R_{\text{ext}} = \mathbb{H}\frac{2\tan(\frac{\xi+\alpha}{2}) - \tan(\frac{\alpha}{2})(1-\tan^2(\frac{\xi+\alpha}{2}))}{1-\tan^2(\frac{\xi+\alpha}{2}) + 2\tan(\frac{\xi+\alpha}{2})\tan(\frac{\alpha}{2})}} \tag{9}$$

where

$$\tan\left(\frac{\xi+\alpha}{2}\right) = \frac{\tan(\gamma)+\tan(\theta)}{1-\tan(\gamma)\tan(\theta)}\cos\left(\frac{\pi}{m}\right) \tag{10}$$

$$\tan(\gamma) = \tan\left(\frac{\alpha}{2}\right)\cos\left(\frac{\pi}{m}\right) \tag{11}$$

$$\tan(\theta) = \frac{\sqrt{\sin^2(\frac{\beta}{2}) - \sin^2(\frac{\alpha}{2})\sin^2(\frac{\pi}{m})}}{\cos(\frac{\beta}{2})} \tag{12}$$

and m is the number of supplementary FSO transceivers set around the principal FSO transceiver.

We can remark that R_{ext} and thus L_J depend on α, β and m. Hereafter, R_{ext} is sometimes denoted by $R_{\text{ext}}(\alpha, m, \beta)$ and L_J by $L_J(\alpha, m, \beta)$ to express these dependencies.

III. PROBLEM OF DESIGNING MINIMAL COST HAP NETWORK

There are several costs in a HAP network, such as investment, energy, and maintenance costs. Based on the expected life duration and maintenance cycle of a HAP, these costs can be distributed by day as 1) daily amortization cost representing investment cost, 2) average daily maintenance cost, and 3) daily energy cost. Consequently, the problem of minimizing network cost becomes minimizing the daily network cost, which comprises these three components.

Following variables are introduced for formulating mathematically the daily network cost:

- K: Number of HAPs in the network. The HAPs are indexed by $i \in 1..K$.
- n_i^{iF}: Number of FSO transceivers used on HAP$_i$ for inter-HAP communications.
- n_i^{sF}: Number of *serving* FSO transceiver of HAP$_i$.

Let ζ_{H}^{day} and ζ_{F}^{day} be constants that express the daily amortization costs of a HAP and an FSO transceiver, respectively. These costs are defined as the ratio of the prices of the HAP or FSO transceiver to their expected lifetime duration. Then, the overall *daily amortization cost* of the HAP network is:

$$K\zeta_{\text{H}}^{day} + \left(\sum_{i=1}^{K} n_i^{\text{sF}} + \sum_{i=1}^{K} n_i^{\text{iF}}\right)\zeta_{\text{F}}^{day} \tag{13}$$

To evaluate the daily maintenance and energy costs, we need to consider the HAP design. HAPs are classified into two categories based on the underlying physical principle that provides the lifting force for the HAPs: aerodynamic (the HAP is heavier than air) and aerostatic (the HAP is lighter than air). While aerostatic platforms use buoyancy to float in the air, aerodynamic platforms use dynamic forces created by movement through the air [10]. In general, both aerostatic and aerodynamic systems require a "flying energy" to keep the HAP relatively stable for maintaining FSO communication between HAPs and that between HAPs and FSO ground nodes. An aerodynamic system requires a large propulsion power to move. Aerostatic systems typically consume less energy than aerodynamic systems do. To be able to operate for a long duration in space, HAPs are mainly unmanned.

HAPs are equipped with different energy resources such as onsite production (e.g., solar energy harvested by solar panels) or rechargeable energy (e.g., batteries or fuel cells brought from the ground). Solar energy-based HAPs can operate continuously in space until they are lowered for maintenance purpose. Rechargeable energy-based HAPs are lowered once the reserved energy is depleted. In brief, the continuous in-space working duration of a HAP is limited by its available energy, which is relatively fixed by the HAP design, its energy consumption level, which varies depending

TABLE 1. Parameters.

Parameter notations	Descriptions	Values	References
	Cost related parameters		
ζ_{H}^{day}	Daily amortization cost of a HAP.	100	
ζ_{F}^{day}	Daily amortization cost of an FSO transceiver on HAP.	10	
ζ^{mtn}	Cost of one-time maintenance of a HAP including lowing it down, maintenance, charging and reinstall it in the stratosphere.	1000	
$\mathbb{D}^m$	Maintenance cycle.	365 days	[6]
	Energy parameters		
$\mathbb{E}^{solar}$	Minimum daily harvested solar energy by a HAP.	42 kWh - 290 kWh	[16]
ρ^{avion}	Power consumed by the avionic part of a HAP to carry one unit of mass.	2 W/kg	
$\rho_{\mathrm{F}}^{\mathrm{HCM}}$	Power for heating, cooling, and management for each FSO on HAP.	20 W	[7]
ρ^{PAT}	Power consumed by a Pointing Acquisition and Tracking (PAT) system.	15W	[17]
$\rho_{\mathrm{F}}^{inter}$	Power consumed by an inter-HAP FSO transceiver for laser source (0.1 W), heating/cooling/management (20 W) and PAT (15 W).	35.1 W	[7]
	Inter-HAP FSO link parameters		
C_n^2	Atmosphere structure parameter.	$5.0 \times 10^{-18} m^{-2/3}$	
σ	Attenuation coefficient.	$3.5 \times 10^{-6} m^{-1}$	[7]
-	Coupling loss.	45 dBm	
-	Transmitted power of an inter-HAP FSO transceiver.	0.1 W	[7]
-	Receiver aperture diameter of an inter-HAP FSO transceiver.	0.037 m	[7]
-	Beam width of an inter-HAP FSO transmitter.	280 μrad	[7]
	HAP-ground link parameters and variables		
σ	Attenuation coefficient.	$3.5 \times 10^{-6} m^{-1}$	
$\rho_{\mathrm{tx}}^{\mathrm{FSO}}$	Transmitted power of the laser source of a *serving* FSO transceiver.	1 Watt	
$\mathbb{R}_{\mathrm{rx}}$	Receiver telescope aperture radius of a ground FSO transceiver.	0.75m	[15]
-	Power threshold of a ground FSO receiver	-50.9 dBm	[7]
-	Power margin of a ground FSO receiver	1.2 dBm	
ρ_{rx}	Required received power at a ground FSO transceiver.	-49.62 dBm (or $1.09 \times 10^{-}8$ W)	
	Other parameters		
$\mathbb{H}$	Elevation of HAPs.	20 km	
L^{HH}	Maximum allowable length of an inter-HAP link so that its Bit error rate (BER) is under δ.	87 km	
δ	BER threshold for inter-HAP links and lightpaths between HAPs.	10^{-3}	
$\mathbb{W}$	The number of wavelengths per FSO link according to used WDM technique.	40; 80	
μ_{H}	Platform mass excluding FSO transceivers.	28.5 kg; 500 kg	[7]
μ_{F}	FSO transceiver mass.	6.3 kg	[7]

on the payload weight and communication of the HAP, and its maintenance cycle.

We define the *maintenance cost* of a HAP as the expense of lowering the HAP to perform technical maintenance, energy recharge on the ground, and then reinstall it in space.

Let d_i be the number of days on which HAP$_i$ can operate continuously in space. Let ζ^{mtn} be constant expressing the cost of one time lowering a HAP, maintaining it, recharging it, and then reinstalling it in space. The *daily maintenance cost* of the HAP network is

$$\sum_{i=1}^{K} \frac{\zeta^{mtn}}{d_i} \tag{14}$$

Regarding the *daily energy cost*, we consider solar energy to be free, whereas the solar panel cost is counted in the cost of the HAP. The cost of rechargeable energy is part the maintenance cost. As a result, the energy cost does not explicitly present in the total cost. Nonetheless, the energy consumption level of a HAP affects its in-space working duration d_i; therefore, we analyze this in Section IV.

Combining (13) and (14), and let denote the overall daily cost of the HAP network by ζ, then:

$$\zeta = K\zeta_{\mathrm{H}}^{day} + \left(\sum_{i=1}^{K} n_i^{\mathrm{sF}} + \sum_{i=1}^{K} n_i^{\mathrm{iF}}\right)\zeta_{\mathrm{F}}^{day} + \sum_{i=1}^{K} \frac{\zeta^{mtn}}{d_i} \tag{15}$$

The problem of minimizing daily cost of the HAP network is stated as follows.

- Given input parameters including
  - $\mathbb{N}_{\mathrm{FSO}}$: Set of ground FSO nodes and their coordinates. The number of nodes in the set is denoted as $|\mathbb{N}_{\mathrm{FSO}}|$,
  - $\mathbb{M}$: Data traffic to be carried between ground FSO nodes. This is the list of bandwidth demands between the ground nodes.
- Outputs to seek are
  - A HAP network with HAP locations and inter-HAP links,
  - Beam width to set to each *serving* FSO transceiver.
- Optimization objective is
  - Minimizing the daily cost expressed in (15) of the HAP network.

The following two remarks drive us to conduct further analyses in subsequent sections. First, if a HAP has self-sufficient solar energy, its in-space working duration d_i is not limited by its energy consumption but depends uniquely on the maintenance cycle of the HAP, which is usually constant. In Section IV, we show the daily energy consumption of a HAP and the constraint that a HAP needs to respect to rely solely on solar energy.

Second, the cost of the HAP network increases with an increase in the number of FSO transceivers and HAPs.

The number of HAPs can be reduced by increasing ground coverage. To increase ground coverage, more *serving* FSO transceivers can be used on each HAP, but this introduces greater energy consumption and extra amortization cost. Section V focuses on identifying the optimal configuration for *serving* FSO transceivers on a HAP to achieve a minimal HAP network cost.

IV. DAILY ENERGY CONSUMPTION OF A HAP WITH PAYLOAD

Several parameters affect the power consumption of a HAP. The descriptions and notations of these parameters are listed in section Energy parameters of Table 1. Most parameters were set based on industrial experimental projects such as the Loon project [7], Stratobus project [6], and other studies listed in the reference column. Section VII-A presents the choice of parameter values in detail.

Let us consider the power consumption of a single HAP H_i that has m *serving* FSO transceiver and n_i^{iF} inter-HAP FSO transceivers. The power consumption includes:

- $P_{H_i}^{avion}$: Power draw of avionic part for maintaining H_i with payload in space.
- $P_{H_i}^{down}$: Power draw of all *serving* FSO transceivers on HAP H_i. This power includes the heating/cooling/management power, laser transmitted power of all *serving* FSO transceivers on the HAP, and the power consumed by the Pointing Acquisition and Tracking (PAT) system of the HAP.
- $P_{H_i}^{inter}$: Power draw of all inter-HAP FSO transceivers on HAP H_i for inter-HAP communication. The power includes the heating/cooling/management, and PAT power for each inter-HAP FSO transceiver. Inter-HAP FSO transceivers are oriented towards different remote HAPs; therefore, each transceiver must have a PAT system.

The total daily energy consumption (by 24 hours) of H_i is

$$\mathbb{E}^{consum} = (P_{H_i}^{avion} + P_{H_i}^{down} + P_{H_i}^{inter}) \times 24 \tag{16}$$

To breakdown further $P_{H_i}^{avion}$, $P_{H_i}^{down}$, and $P_{H_i}^{inter}$, we introduce following parameters:

- ρ^{avion}: Power consumed by the avionic part of the HAP to carry a unit of mass.
- $\rho_{\mathrm{tx}}^{\mathrm{FSO}}$: Transmitted power of each *serving* FSO transceiver. Because the current power of laser source is limited to 1 W, which is very small in comparison with the power consumed by other factors on the HAP, we consider that $\rho_{\mathrm{tx}}^{\mathrm{FSO}} = 1$ W, regardless of the beam width of the *serving* FSO transceiver.
- $\rho_{\mathrm{F}}^{\mathrm{HCM}}$: Power draw for heating, cooling, and management. It is also considered constant for each *serving* FSO transceiver and is set to $\rho_{\mathrm{F}}^{\mathrm{HCM}} = 20$ W, according to reference [7].
- ρ^{PAT}: Power draw for Pointing, Acquisition and Tracking activity; it is another constant and is set to $\rho^{\mathrm{PAT}} = 15$ W [17]. A HAP system uses a single PAT for its set of *serving* FSO transceivers.
- $\rho_{\mathrm{F}}^{inter}$: Power draw of a single inter-HAP FSO transceiver including communication, heating, cooling, management, and PAT. According to [7], with inter-HAP link parameters as given in Table 1, 0.1 W laser power is sufficient for an inter-HAP communication of 100 km distance. In this study, we limited the inter-HAP link length to 87 km and considered the laser power constantly 0.1 W regardless of the distance. Therefore, $\rho_{\mathrm{F}}^{inter} = \rho_{\mathrm{F}}^{\mathrm{HCM}} + \rho^{\mathrm{PAT}} + 0.1$.
- μ_{H}: Mass of the HAP.
- μ_{F}: Mass of an FSO on the HAP.

Assuming that $P_{H_i}^{avion}$ is linearly proportional to the weight of the HAP by ρ^{avion},

$$P_{H_i}^{avion} = [\mu_{\mathrm{H}} + (n_i^{\mathrm{sF}} + n_i^{\mathrm{iF}})\mu_{\mathrm{F}}]\rho^{avion} \tag{17}$$

$P_{H_i}^{down}$ is the sum of the power consumed by *serving* FSO transceivers and PAT activity of the HAP; thus,

$$P_{H_i}^{down} = n_i^{\mathrm{sF}}(\rho_{\mathrm{tx}}^{\mathrm{FSO}} + \rho_{\mathrm{F}}^{\mathrm{HCM}}) + \rho^{\mathrm{PAT}} \tag{18}$$

$P_{H_i}^{inter}$ is the sum of the power consumed by inter-HAP FSO transceivers; thus,

$$P_{H_i}^{inter} = \rho_{\mathrm{F}}^{inter} n_i^{\mathrm{iF}} \tag{19}$$

Substituting (17), (18), and (19) into (16), we obtain the daily power consumption of a HAP as

$$\begin{aligned}\mathbb{E}^{consum} = \{&[\mu_{\mathrm{H}} + (n_i^{\mathrm{sF}} + n_i^{\mathrm{iF}})\mu_{\mathrm{F}}]\rho^{avion} \\ &+ n_i^{\mathrm{sF}}(\rho_{\mathrm{tx}}^{\mathrm{FSO}} + \rho_{\mathrm{F}}^{\mathrm{HCM}}) + \rho^{\mathrm{PAT}} \\ &+ \rho_{\mathrm{F}}^{inter} n_i^{\mathrm{iF}}\} \times 24\end{aligned} \tag{20}$$

A. NECESSITY OF SOLAR ENERGY AND UTILIZATION CONSTRAINT

Current HAPs mainly use energy from solar panels mounted on HAP wings and/or energy from batteries or hydrogen fuel cells (HFC) onboard. Solar energy can be harvested and charged into batteries during the day for nighttime use. Harvested solar energy varies with year time and location. According to the experiments in [16], in York, UK, the harvested solar power is 42–80 kWh/day, and in Enugu, Nigeria, it is 290–545 kWh/day, depending on the size of the solar panel.

Figure 7 depicts the total daily energy consumption of a HAP, calculated from (20), versus the number of *serving* FSO transceivers. Parameters were $\rho^{avion} = 2$ W/kg, $\rho^{\mathrm{PAT}} = 15$ W, HAP weights $\mu_{\mathrm{H}} = 28.5$ kg or 500 kg. The HAP carried 10 inter-HAP FSO transceivers. The referenced daily solar energy levels were the minimum daily solar energy levels in York and Enugu. From a certain number of *serving* FSO transceivers, a HAP consumes more energy than the harvested solar energy in York, and an HFC would be necessary. Owing to the limited payload capacity of a HAP, its HFC capacity is also very limited. According

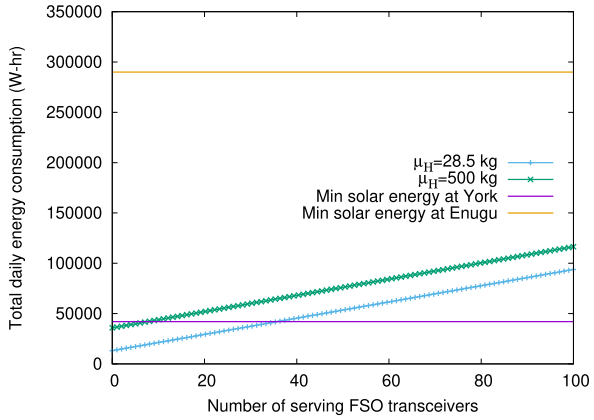

FIGURE 7. Energy consumption by a HAP with different number of serving FSO transceivers in comparison with the minimum harvested solar energy at York and Enugu. $\rho^{avion} = 2/kg$ W and $\rho^{\text{PAT}} = 15$ W.

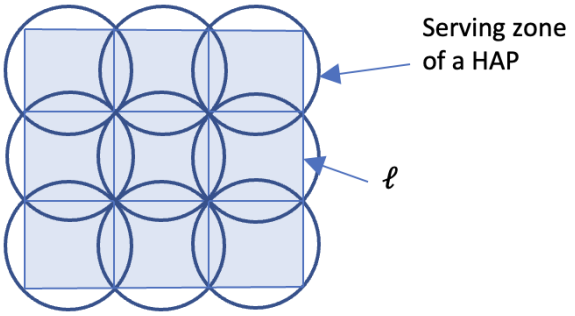

FIGURE 8. A ground area is divided into grid of square cells; each cell is circumscribed by a circle representing a serving zone of a HAP.

to [10], the current state-of-the-art fuel-cell density is approximately 1600 Wh/kg. A lightweight HAP, such as a Google balloon weights 28.5 kg, cannot carry heavy long-lasting fuel cells on board. The larger HAP Stratobus can carry up to 450 kg, but it weights already 7 tons leading to high energy consumption for flying. Even if the Stratobus payload capacity is reserved for the HFC, its energy would quickly run out within a few days.

Based on this observation, we believe that *long-duration flights should consider solar energy as the principal energy source*. In this case, the power consumption of a HAP with payload must not exceed the daily harvested solar energy. Let the daily harvested solar energy be $\mathbb{E}^{solar}$; then,

$$\Big([\mu_{\text{H}} + (n_i^{\text{sF}} + n_i^{\text{iF}})\mu_{\text{F}}]\rho^{avion} + \rho^{\text{PAT}} + n_i^{\text{sF}}(\rho_{\text{tx}}^{\text{FSO}} + \rho_{\text{F}}^{\text{HCM}}) + \rho_{\text{F}}^{inter} n_i^{\text{iF}}\Big) \le \frac{\mathbb{E}^{solar}}{24} \quad (21)$$

According to Figure 7, solar energy provision does not need to be very large. A solar energy level between the minimum harvested in York and Enugu allows a 500 kg HAP to carry at least 6 *serving* FSO transceivers. A HAP can carry hundreds FSO transceivers with more than 125 kWh solar energy. Therefore, it is realistic to rely on the solar energy. Hereafter, we consider that HAPs solely use solar energy.

Despite self-sufficient solar energy, HAPs still need to be lowered periodically for maintenance, for example, after one year in the case of Stratobus [6]. Let us denote the maintenance cycle as a constant $\mathbb{D}^m$. Then

$$d_i = \mathbb{D}^m, \qquad \forall i \in 1..K \quad (22)$$

V. OPTIMAL *m*FSO CONFIGURATION

Using multiple *serving* FSO transceivers increases the expense of FSO transceivers, although it can reduce the expense regarding HAPs. This section aims to determine the *m*FSO configuration that minimizes the HAP network cost defined in (15). We assume that all HAPs use identical *m*FSO configurations, that is, identical principal beam width α, supplementary beam width β and number of supplementary *serving* FSO transceivers m.

Let us now consider the dependence of the HAP network cost on *m*FSO configuration. As each HAP has a principal *serving* FSO transceiver, m supplementary *serving* FSO transceivers and uses only solar energy, the cost (15) becomes

$$\zeta = K\zeta_{\text{H}}^{day} + \left[K(m+1) + \sum_{i=1}^{K} n_i^{\text{iF}}\right]\zeta_{\text{F}}^{day} + \frac{K\zeta^{mtn}}{\mathbb{D}^m}$$

ζ is a function of K, m and n_i^{iF}. K depends on the coverage radius $R_{\text{ext}}(\alpha, m, \beta)$ of the *m*FSO configuration. n_i^{iF}, as the number of inter-HAP links of HAP i, depends on the traffic demand set $\mathbb{M}$. Hence, ζ depends on *m*FSO configuration and $\mathbb{M}$. It is difficult to determine the optimal *m*FSO configuration without considering $\mathbb{M}$. To relax the dependance on $\mathbb{M}$, we estimate ζ by a function that depends solely on *m*FSO configuration, that is, tuple (α, m, β); then try to find an instance (α, m, β) minimizing the estimated cost in expecting that the instance also drives the real cost to a minimum.

A. COST ESTIMATION

First, we estimate the number of HAPs K. Samples of the estimation are datasets with uniformly distributed ground nodes. Let S be the surface of the ground area containing those nodes, and $\mathbb{W}$ the number of wavelengths in the WDM technique. We divide the ground zone S into a grid of square cells of size $\ell \times \ell$, each one will be covered by a HAP (see Figure 8). To be served by a HAP, a cell must satisfy the following two conditions:

1) A cell can contain at most $\mathbb{W}$ ground nodes because a HAP can use at most $\mathbb{W}$ wavelengths to serve ground nodes. Owing to the uniform distribution of ground nodes, we have
$$\frac{\ell^2}{S}|\mathbb{N}_{\text{FSO}}| \le \mathbb{W}$$
2) A cell must be contained inside by a circle radius equivalent to the extended radius R_{ext} of a HAP
$$\ell \le \sqrt{2}R_{\text{ext}}$$

The maximum number of HAPs required to cover region S is the number of cells. Let this number be $\hat{K}$, then,

$$\hat{K} = \frac{S}{\ell^2} = \left\lceil \max\left\{ \frac{|\mathbb{N}_{\text{FSO}}|}{\mathbb{W}}, \frac{S}{2R_{\text{ext}}^2} \right\} \right\rceil \tag{23}$$

Hence, $\hat{K}$ is an overestimation of the number of HAPs.

Next, we estimate the value of n_i^{iF}. Let $\mathbb{V}$ be the maximum number of inter-HAP links that a HAP may have. Then

$$n_i^{\text{iF}} \leq \mathbb{V}, \forall i.$$

Finally, ζ can be overestimated by $\widehat{\zeta}$ as follows:

$$\widehat{\zeta} = \hat{K}\left[\zeta_{\text{H}}^{day} + (m + \mathbb{V} + 1)\zeta_{\text{F}}^{day} + \frac{\zeta^{mtn}}{\mathbb{D}^m}\right] \tag{24}$$

$\widehat{\zeta}$ is a function of $R_{\text{ext}}(\alpha, m, \beta)$ and m while $\mathbb{V}$ is a parameter of the estimator. The estimation is more precise when $\mathbb{V}$ is set close to the actual number of inter-HAP links of a HAP, and coarser otherwise.

B. ALGORITHMS FINDING OPTIMAL CONFIGURATION

Given α and m, a larger β results in a larger R_{ext}, and thus a smaller $\hat{K}$ and $\widehat{\zeta}$. Therefore, β should be set to the largest value according to (7) for a given α and m. It is worth noting that the value of β does not affect the solar energy consumption because laser power $\rho_{\text{tx}}^{\text{FSO}}$ (which is P_{tx} in Eq. 7) is small and is considered constant. Determining the optimal configuration becomes finding the optimal values of α and m.

Algorithm 1 Find the Optimal mFSO Configuration

```
function Find-optimal-mFSO
    n_i^iF ← 𝕍
    cMin ← ∞                                   ▷ cost min
    αMax ← maximum α by (4)
    for α = αMax ... 0 do
        mMax ← calculated by (25)              ▷ max m
        mOpt ← 0                               ▷ optimal m
        for m = 0 ... mMax do
            β ← Beta-max(α, m)                 ▷ max β
            Calculate R_ext(α, m, β) using (9),(10),(11) (12)
            Calculate ζ̂(α, m, β) using (24)
            if ζ̂ < cmin then
                cmin ← ζ̂
                αOpt ← α                       ▷ optimal α
                mOpt ← m                       ▷ optimal m
                βOpt ← β                       ▷ optimal β
            end if
        end for
    end for
    return αOpt, mOpt, βOpt
end function
```

Following an exhaustive search approach, we examine all possible values of α and m to seek for the pair that minimizes $\widehat{\zeta}$ in (24). The search range of α is from 0° to the maximum value set by constraint (4). The number of supplementary *serving* FSO transceivers m is also limited. Indeed, since the number of inter-HAP links of a HAP can go up to $\mathbb{V}$ as set in Section V-A, and $n_i^{\text{sF}} = m + 1, \forall i$, then from the energy constraint (21), we deduce the upper bound for m:

$$m \leq \frac{\frac{\mathbb{E}^{solar}}{24} - (\mathbb{V}\mu_{\text{F}}\rho^{avion} + \mathbb{V}\rho_{\text{F}}^{inter} + \mu_{\text{H}}\rho^{avion} + \rho^{\text{PAT}})}{\mu_{\text{F}}\rho^{avion} + \rho_{\text{F}}^{\text{HCM}} + \rho_{\text{tx}}^{\text{FSO}}} - 1 \tag{25}$$

Algorithm 2 Find the Maximum β Given α, m

```
function Beta-max(α, m)
    for β = 0 ... 180 do
        Calculate R_ext(α, m, β) using (9),(10),(11) (12)
        Calculate L_J using (8)
        Calculate P_J^rx using (6)
        if P_J^rx < ρ_rx then ▷ Looking for the first β violate constraint (7)
            return β-1 ▷ the previous trial β was the maximum
        end if
    end for
end function
```

Algorithm 1 implements the exhaustive search idea. First, two nested loops scan all possible values of α satisfying constraint (4) and all possible values of m satisfying (25) to find the pair that minimizes $\widehat{\zeta}$ in (24). For each pair (α, m), the largest value of β according to constraint (7) is selected using Algorithm 2. The optimal mFSO configuration is reported by the algorithms as $(\alpha Opt, mOpt, \beta Opt)$.

Algorithm 2 finds the maximum β that satisfies constraint (7) for a given pair of (α, m) by testing the possible values of β increasingly from 0 until the received power P_J^{rx} at the border of the extended coverage area reaches the required received power ρ_{rx}. The received power P_J^{rx} is calculated using the set of equations (6), (8), (9),(10),(11), and (12).

In the implementation of both algorithms, α and β step by 1∘ after each iteration. Finer stepping allows obtaining more accurate results. However, even with 1° stepping, the variation in the optimal R_{ext} is only a few hundred meters, which is negligible in comparison to the absolute value of R_{ext} which is in the range of 6-20 kilometers.

The complexity of Algorithm 1 is $O(m)$ because $\alpha \leq \pi$. The complexity of Algorithm 2 is constant because $\beta \leq \pi$.

VI. DESIGN HAP NETWORK TOPOLOGY

This section presents the HAP network design using the optimal configuration identified above. Let denote L^{inter} as the number of inter-HAP links. Since $\sum_{i=1}^{K} n_i^{\text{iF}}$ is the total number of inter-HAP FSO transceivers, it is equal to 2L^{inter}. The network cost becomes:

$$\zeta = K\zeta_{\text{H}}^{day} + [K(m+1) + 2\text{L}^{inter}]\zeta_{\text{F}}^{day} + K\frac{\zeta^{mtn}}{\mathbb{D}^m}$$

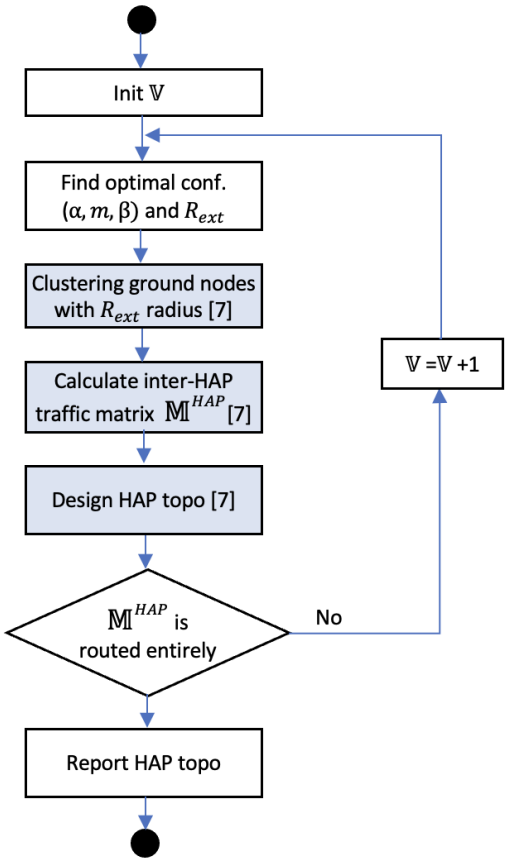

FIGURE 9. HAP network design flowchart.

and is equivalent to

$$\zeta = K\left[\zeta_{\mathrm{H}}^{day} + (m+1)\zeta_{\mathrm{F}}^{day} + \frac{\zeta^{mtn}}{\mathbb{D}^m}\right] + 2\mathrm{L}^{inter}\zeta_{\mathrm{F}}^{day} \quad (26)$$

The cost is proportional to the number of HAPs K and the number of inter-HAP links L^{inter}. We consider that the daily amortization cost of a HAP is much greater than that of an FSO transceiver; thus, the coefficient of K is much greater than the coefficient of L^{inter} in ζ. Consequently, K should be prioritized to minimize over L^{inter}. Therefore, the topology design is broken into following two steps:

i) ground nodes are clustered into equal radius circles that will become serving zones of HAPs in such a way that the number of clusters is the smallest for minimizing K;
ii) corresponding HAPs are located at the centers of clusters but at an elevation of 20 km and are interconnected by the fewest number of inter-HAP links, L^{inter}.

A HAP network topology design algorithm was proposed in [9] following these two steps. In this algorithm, the clustering radius was not determined but was left as an input of the algorithm. In the current study, we set the clustering radius as the extended coverage radius R_{ext} of the optimal mFSO configuration to drive towards a HAP network with minimal ζ. The main steps of the HAP network design process are presented in Figure 9, where the steps taken from [9] are shown in color. The process is explained as follows:

- Initialize $\mathbb{V}$, the maximum number of inter-HAP links of a HAP, by a constant.
- Calculate the optimal mFSO configuration using Algorithm 1, and set its R_{ext} as the clustering radius.
- Apply the clustering algorithm proposed in [9] to distribute ground nodes into clusters of radius R_{ext} while keeping the number of ground nodes in each cluster under $\mathbb{W}$. Each cluster becomes a serving zone of a HAP. The HAP is located at the center of the cluster but at an elevation of 20 km.
- Bandwidth demands between ground nodes belonging to different serving zones are bundled into lightpaths between corresponding HAPs, creating the inter-HAP traffic matrix $\mathbb{M}^{HAP}$.
- Apply HAP topology design algorithm proposed in [9] to build the HAP topology. The algorithm begins with an empty topology. It finds a route for each lightpath demand of $\mathbb{M}^{HAP}$ from a full-mesh graph linking all HAPs within communication distance limit L^{HH}. Whenever a lightpath uses an inter-HAP link that has not yet been included in the current HAP topology, the link is incorporated into the topology. The link in the topology is prioritized for use in building routes for the next lightpath demands.
- Once all lightpath demands in $\mathbb{M}^{HAP}$ are routed, the final topology is achieved. Otherwise, routing may fail due to the low connectivity between HAPs. In this case, $\mathbb{V}$ is increased by one, and the process is repeated until all lightpath demands in $\mathbb{M}^{HAP}$ are routed.

VII. SIMULATION RESULTS

The algorithms for finding the optimal mFSO configuration were implemented and integrated with the topology designed algorithm described in Section VI. We performed simulations with practical parameters and evaluated the efficiency of mFSO configuration compared to the single *serving* FSO transceiver configuration.

A. PARAMETER VALUES

The simulation parameters are listed in Table 1. The values of these parameters were chosen according to experiments reported in the literature. This subsection explains the choices of the parameter values.

Cost-related parameters: The cost-related parameters are set such that the daily amortization cost of a HAP is significantly greater than that of an FSO transceiver, and the one-time maintenance cost is significantly higher than the daily amortization cost of a HAP. The maintenance cycle of a HAP is set as $\mathbb{D}^m = 1$ year according to published information on Stratobus [6].

Energy-related parameters:

- $\mathbb{E}^{solar}$: we considered daily solar energy levels between the minimum daily solar energy values in York and

Enugu reported in [16], which were 42 kWh and 290 kWh, respectively.

- ρ^{avion}: although the power-to-mass ratio can be estimated as 6 W/kg according to [16], the published power rates of real systems are smaller. For aerodynamic systems such as Zephir-S, Zephir-T [18], and Phasa-35 [19], ρ^{avion} varies from 2.68 -3.04 W/kg. Indeed, Zephir-S weighs 80 kg (75 kg platform and 5 kg payload) and consumes 243 W, Zephir-T weighs 160 kg (140 kg platform and 20 kg payload) and consumes 429 W, and Phasa-35 weighs 165 kg (150 kg platform and 15 kg payload) and consumes 459 W. Aerostatic systems consume even less power. The Stratobus weighs 7000 kg and consumes 5 kW when it carries a 250 kg payload and 8 kW when it carries 450 kg [6]. Thus, the power-to-mass ratio of Stratobus is between 0.69 and 1.07 W/kg only. Therefore, in this simulation ρ^{avion} was set to 2 W/kg.
- ρ^{PAT} was set to 15 W according to [17].
- $\rho_{\text{F}}^{\text{HCM}}$ was set to 20 W according to [7].
- ρ_{F}^{inter} was set to 35.1 W including laser power, $\rho_{\text{F}}^{\text{HCM}}$ and ρ^{PAT}.

Inter-HAP link parameters: were used to calculate the Bit error rate (BER) of the link and were set based on parameters of the Loon project [7]. The inter-HAP link is modeled as a Gamma-Gamma distribution turbulence channel. Its BER is calculated based on the mathematical models shown in Section III.B of [20].

HAP-ground FSO link parameters: The attenuation coefficient of an FSO link between a HAP and a ground node is set identical to that of inter-HAP links. The telescope aperture radius $\mathbb{R}_{\text{rx}}$ of a ground FSO receiver was set to 0.75 m as the telescope presented in [15]. Large size telescopes are not used for FSO receivers on HAPs. The required received power was set to $\rho_{\text{rx}} = -49.62$ dBm so that with margin 1.2 dBm, the received power is still higher than the power threshold -50.9 dBm set in [7].

Other parameters:

- δ was set to 10^{-3} because errors with that BER can be corrected using current Forward Error Correction (FEC) techniques.
- L^{HH} was set to 87 km so that the BER of an inter-HAP link limited by L^{HH} is under δ.
- μ_{H} varies significantly from one HAP design to another. The Loon balloon weighs just 28.5 kg while the Stratobus weighs 7000 kg. With $\rho^{avion} = 2$ W/kg, a HAP weighing more than 7000 kg already consumes 326 kWh/day to carry itself, which is more than the maximum harvested solar energy, leading to lacking energy to carry FSO transceivers. Therefore, $\mu_{\text{H}} = 500$ kg was used in the simulations.
- μ_{F} was set according to the FSO transceiver used in the Loon project, which weighs 6.3 kg [7]. This value is consistent with the weights between 8 and 10 kg of commercial terrestrial SONABeam FSO transceivers [1].

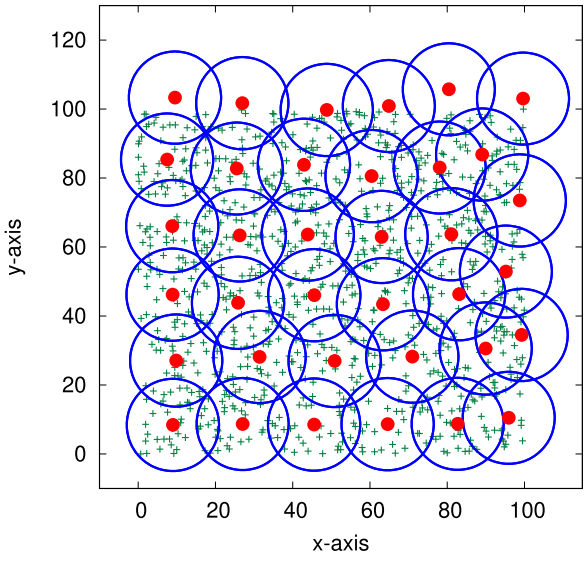

FIGURE 10. Footprints of HAPs with *m*FSO configuration obtained from the topology design for a test case of 1005 ground FSO nodes when $\mathbb{E}^{solar} = 75$ kwh, $\mathbb{W} = 80$. A circle represents an extended coverage area of a HAP. Small points inside the circle are ground nodes and the dot at the center of the circle is the projected location of its serving HAP on the ground.

- $\mathbb{W}$ was set to 40 or 80 according to the current WDM technique.

The test dataset contained 19 test cases, each with 400 – 2800 ground nodes. The ground FSO node locations were randomly generated on a square surface of 100 × 100 km, which is the size of a large metropolis. The test cases had different numbers of ground nodes, reflecting different ground node densities. The traffic requirement $\mathbb{M}$ contained demands randomly generated between ground FSO nodes such that the total incoming or outgoing traffic of a ground FSO node did not exceed 1 Gbps, which is the capacity of a single wavelength.

Initially, $\mathbb{V}$ was set to 10. The optimal multiple *serving* FSO transceiver configuration (α, m, β) was calculated using Algorithms 1 and 2. The extended radius R_{ext} of the optimal configurations was calculated using (9) and was then used as the clustering radius in the HAP topology design step.

With $\mathbb{E}^{solar} = 42$ kWh and $\mathbb{W} = 40$, $\mathbb{V}$ must be increased to 12 to get all demands in $\mathbb{M}^{HAP}$ routed successfully for all test cases. With all other $\mathbb{E}^{solar}$ and $\mathbb{W}$ values, the topology design algorithm successfully routed all demands in $\mathbb{M}^{HAP}$ for all test cases right with initial $\mathbb{V} = 10$.

Figure 10 illustrates the HAP locations and their footprints calculated using the proposed algorithms for a test case of 1005 ground FSO nodes, $\mathbb{E}^{solar} = 75$ kWh, and $\mathbb{W} = 80$.

B. *m*FSO CONFIGURATION VERSUS SINGLE SERVING FSO TRANSCEIVER CONFIGURATION

Table 3 lists the maximum beam width α_{max} according to (4) and the maximum ground coverage radius of the single

TABLE 2. Optimal configurations and costs of all test cases with receiver telescope aperture radius $\mathbb{R}_{rx}$ = 0.75 m.

	$\mathbb{E}^{solar}$ = 42 kWh										$\mathbb{E}^{solar}$ = 50 ∼ 290 kWh									
	$\mathbb{W}=40, \mathbb{V}=12$					$\mathbb{W}=80, \mathbb{V}=10$					$\mathbb{W}=40, \mathbb{V}=10$					$\mathbb{W}=80, \mathbb{V}=10$				
$\lvert\mathbb{N}_{FSO}\rvert$	α	m	β	R_{ext}	cost ζ	α	m	β	R_{ext}	cost ζ	α	m	β	R_{ext}	cost ζ	α	m	β	R_{ext}	cost ζ
(1)	(2)	(3)	(4)	(5)	(6)	(7)	(8)	(9)	(10)	(11)	(12)	(13)	(14)	(15)	(16)	(17)	(18)	(19)	(20)	(21)
480	37	0	-	6691	15308	37	0	-	6691	13488	37	13	17	11929	10010	37	13	17	11929	9470
588	37	0	-	6691	16639	37	0	-	6691	14519	37	13	17	11929	9304	37	13	17	11929	8964
763	37	0	-	6691	18495	37	0	-	6691	15815	37	13	17	11929	9990	37	13	17	11929	9510
854	37	0	-	6691	19141	37	0	-	6691	16341	37	13	17	11929	10493	37	13	17	11929	9933
998	37	0	-	6691	19101	37	0	-	6691	16701	37	13	17	11929	10855	37	13	17	11929	10215
1005	37	0	-	6691	19068	37	0	-	6691	16308	37	13	17	11929	11138	37	13	17	11929	10478
1150	37	0	-	6691	19666	37	0	-	6691	16926	37	13	17	11929	10915	37	13	17	11929	10275
1345	37	0	-	6691	20644	37	0	-	6691	17564	37	13	17	11929	11741	37	13	17	11929	10395
1477	37	0	-	6691	20752	37	0	-	6691	17612	37	12	17	11539	13115	37	13	17	11929	10335
1523	37	0	-	6691	21895	37	0	-	6691	18595	37	12	17	11539	14053	37	13	17	11929	10375
1675	37	0	-	6691	21735	37	0	-	6691	18535	37	11	17	11042	14128	37	13	17	11929	10495
1736	37	0	-	6691	22461	37	0	-	6691	19301	37	11	17	11042	14874	37	13	17	11929	10455
1911	37	0	-	6691	22481	37	0	-	6691	19021	37	10	17	10395	14869	37	13	17	11929	10495
2009	37	0	-	6691	22641	37	0	-	6691	19321	37	10	17	10395	15575	37	13	17	11929	10595
2135	37	0	-	6691	22761	37	0	-	6691	19221	37	10	17	10395	16493	37	13	17	11929	10575
2304	37	0	-	6691	22881	37	0	-	6691	19301	37	9	17	9524	18192	37	13	17	11929	10655
2325	37	0	-	6691	22368	37	0	-	6691	18948	37	9	17	9524	18555	37	13	17	11929	10675
2491	37	0	-	6691	22761	37	0	-	6691	19401	37	8	18	9524	18660	37	13	17	11929	10655
2753	37	0	-	6691	23346	37	0	-	6691	19926	37	8	18	9524	20284	37	13	17	11929	11178

TABLE 3. Maximum beam width and coverage radius of single *serving* FSO transceiver configuration with different receiver telescope aperture radius.

Receiver telescope aperture radius $\mathbb{R}_{rx}$ (m)	Maximum beam width α_{max}	Maximum coverage radius (m)
0.75	37 °	6691
1	49 °	9114

TABLE 4. Maximum extended coverage radius of *m*FSO configuration when $\mathbb{V}$ = 10 with different receiver telescope aperture radius.

$\mathbb{E}^{solar}$ (kWh)	Max m	Max R_{ext} (m)	
		$\mathbb{R}_{rx}=0.75$ (m)	$\mathbb{R}_{rx}=1$ (m)
42	6	6691	9114
50	16	12174	17016
75	47	13559	18663
100	78	13678	18864
125	109	13711	18920
150	140	13724	18943
175	171	13731	18955
200	202	13735	18962
225	233	13738	18966
250	264	13739	18969
275	295	13740	18971
290	314	13741	18972

serving FSO transceiver configuration when the receiver telescope aperture radius varied. Table 4 lists the extended coverage radius of the maximum *m*FSO configuration for different solar energy levels and receiver telescope aperture radii. The maximum *m*FSO configuration was obtained using the largest principal beam α_{max}, largest m according to (25), and largest β according to (7), given α_{max} and m. The coverage radius of the maximum *m*FSO configuration was extended approximately twice in comparison with that of single FSO transceiver configuration, except for $\mathbb{E}^{solar}$ = 42k Wh. When solar energy level increased, the maximum m increased; thus, the extended coverage radius increased. However, when m was already large, the extension increased slowly with m.

The maximum extended coverage was much larger with $\mathbb{R}_{rx}$ = 1 m than with $\mathbb{R}_{rx}$ = 0.75 m because a larger receiver telescope aperture captures more power thus accepts weaker signal. Therefore, we suggest to use large telescope when it is possible. To keep the simulation appropriate with the existing telescopes, we show only results with receiver telescope aperture radius of $\mathbb{R}_{rx}$ = 0.75 m from now on.

To see how much coverage radius was extended with the optimal *m*FSO configuration, we examined the optimization results in Table 2. The table lists the optimal *m*FSO configurations and network costs. Although the optimal extended coverage radius was smaller than the radius of the maximum configuration, it is still approximately 1.8 times greater than the radius of the single FSO transceiver configuration in many cases (11929 m versus 6691 m) when $\mathbb{E}^{solar} \geq$ 50 kWh.

When $\mathbb{E}^{solar}$ = 42kWh, the optimal number of supplementary *serving* FSO transceivers is m = 0; thus, the configuration uses a single *serving* FSO transceiver. Therefore, these cases were used as references for single *serving* FSO transceiver configuration. When $\mathbb{E}^{solar} \geq$ 50 kWh, all optimal configurations were truly *m*FSO, and the results were identical for all solar energy levels. Cost related numbers indicate that *m*FSO configuration offered significantly lower costs (listed in columns 16^{th} and 21^{th}) than those of single *serving* FSO transceiver configuration (listed in columns 6^{th} and 11^{th}) for the same test cases and number of wavelengths $\mathbb{W}$. The costs resulting from *m*FSO configuration were as low as 54–87% of those resulting from single *serving* FSO transceiver configuration. *These numbers confirm that when there is sufficient solar energy, mFSO configuration is definitively a better choice than single serving FSO configuration.*

C. FACTORS IMPACT OPTIMAL mFSO CONFIGURATION

Comparing the values of the optimal extended coverage radius in Table 2 and the maximum extended coverage radius in Table 4, we can see that the optimal configuration was generally not the maximum. This is reasonable because the

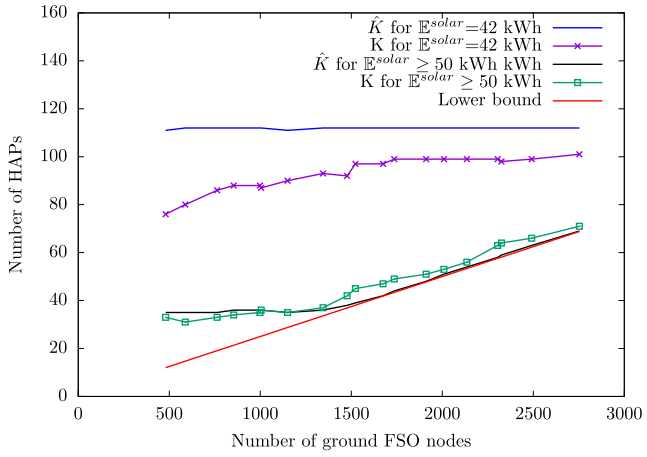

(a) W=40

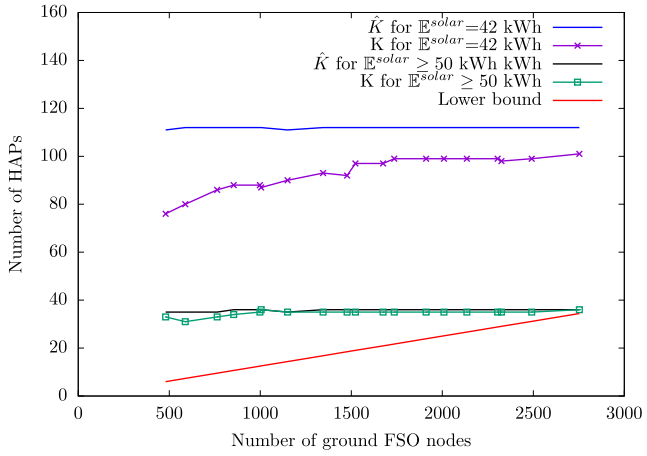

(b) W=80

FIGURE 11. Number of HAPs and lower bound with (a) $\mathbb{W} = 40$ and (b) $\mathbb{W} = 80$ in different solar energy levels.

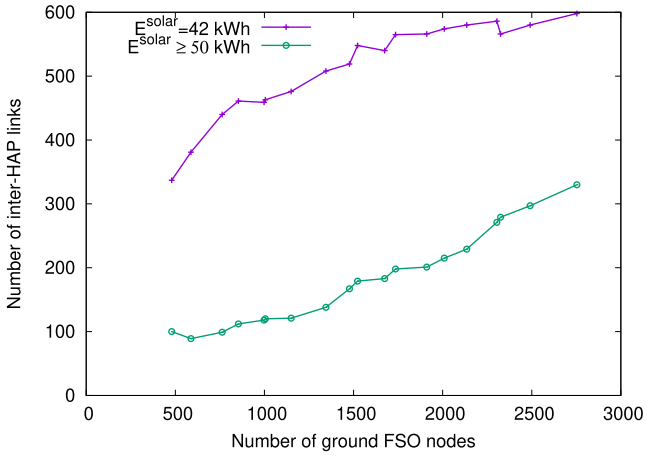

(a) W=40

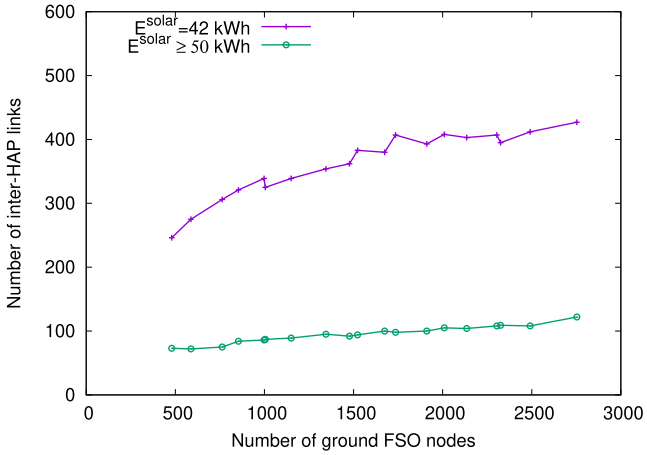

(b) W=80

FIGURE 12. Number of inter-HAP links when (a) $\mathbb{W} = 40$ and (b) $\mathbb{W} = 80$ for different solar energy levels.

maximum configuration uses an excessive number of supplementary *serving* FSO transceivers.

Low solar energy may render *m*FSO configuration impossible. Indeed, $\mathbb{E}^{solar} = 42$ kWh could afford maximally 6 supplementary *serving* FSO transceivers (see Table 4), which was too few to entirely cover the contour of the principal coverage area. Thus, single FSO transceiver configuration was the unique choice.

When the solar energy level exceeds 50 kWh, its exact value does not affect the optimal configuration. The simulation showed that the optimal configurations were identical for all solar energy levels from 50 kWh/day and above. This is explained by the fact that a greater solar energy level allows to accept configurations with large coverage but may be more expensive because of using more supplementary *serving* FSO transceivers. As a result, large configurations were not selected as optimal configurations. *In other words, increasing solar energy does not necessarily improve the HAP network cost.*

Since the optimal multiple *serving* FSO transceiver configurations were identical for all $\mathbb{E}^{solar} \geq 50$ kWh, all other numerical results related to topology design and routing with these solar energy levels were identical and are presented as single results in subsequent figures.

The coverage of the optimal configurations decreased when the ground nodes became denser. Indeed, test cases with large numbers of ground nodes had greater ground node densities, and columns 13^{th} and 15^{th} of Table 2 shows that the optimal m and R_{ext} decreased when the density increased. The reason is that, with a greater ground node density, a small ground region already contains $\mathbb{W}$ ground nodes, which is the maximum serving capacity of a HAP. Therefore, a HAP could serve only a small zone and required only few supplementary FSO transceivers to cover the zone.

D. NUMBERS of HAPs AND INTER-HAP LINKS

Since each HAP can serve at most $\mathbb{W}$ ground FSO nodes, a lower bound for the number of HAPs is:

$$n_{\text{HAP}}^{LB} = \frac{|\mathbb{N}_{\text{FSO}}|}{\mathbb{W}} \tag{27}$$

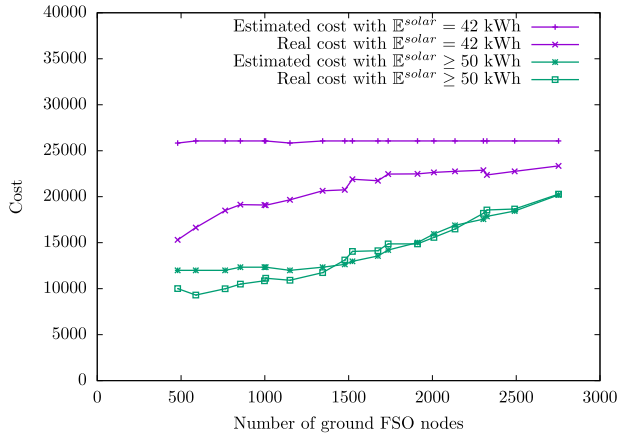

(a) W=40

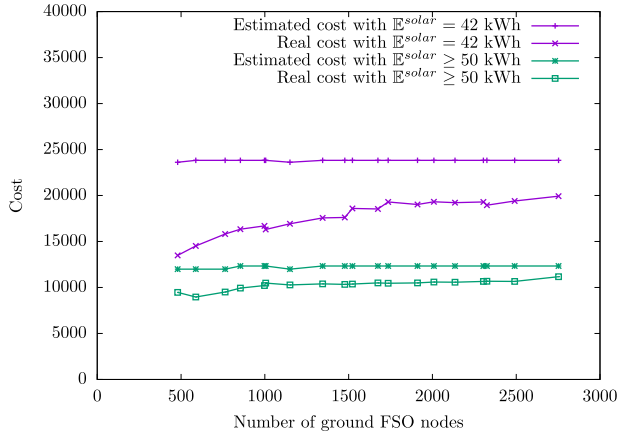

(b) W=80

FIGURE 13. Real costs and overestimated costs with $\mathbb{W} = 40$ and $\mathbb{W} = 80$.

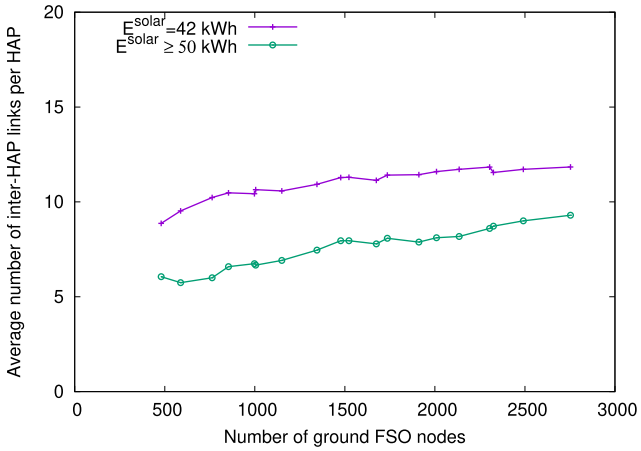

(a) W=40

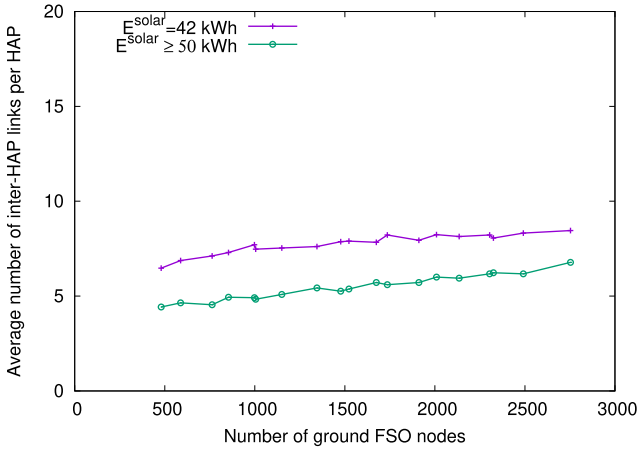

(b) W=80

FIGURE 14. Number of inter-HAP links per HAP when (a) $\mathbb{W} = 40$ and (b) $\mathbb{W} = 80$ for different solar energy levels.

Figure 11 shows the number of HAPs, the estimated number of HAPs $\hat{K}$ and lower bound n_{HAP}^{LB} when (a) $\mathbb{W} = 40$ and (b) $\mathbb{W} = 80$. With $\mathbb{E}^{solar} \geq 50$ kWh, the actual number of HAPs was almost identical to $\hat{K}$ in both subfigures. Furthermore, when $\mathbb{W} = 40$ and $\mathbb{E}^{solar} \geq 50$ kWh, the number of HAPs approached the lower bound starting from test cases with 1000 ground nodes or above. This implies that the number of HAPs was almost optimal.

Figure 12 presents the absolute numbers of inter-HAP links. The number of inter-HAP links increased with the number of ground nodes, because the network size and traffic demand increased. The number of inter-HAP links clearly decreased when the wavelength density increased from $\mathbb{W} = 40$ to $\mathbb{W} = 80$. In other words, denser WDM technique helps reduce the number of inter-HAP FSO transceivers and consequently the network cost.

*m*FSO configuration allows reducing significantly both the numbers of HAPs and inter-HAP links. Indeed, according to Figure 11, the number of HAPs was much smaller with $\mathbb{E}^{solar} \geq 50$ kWh where *m*FSO configuration was used, in comparison with $\mathbb{E}^{solar} = 42$ kWh, where single *serving* FSO configuration was used. A similar phenomenon is observed in Figure 12 for the number of inter-HAP links.

E. QUALITY OF COST ESTIMATION

Figure 13 presents the estimated and actual costs for different solar energy levels and wavelength densities. The estimated cost was very close to the actual cost, mostly for $\mathbb{E}^{solar} \geq 50$kWh and $\mathbb{W} = 40$.

Parameter $\mathbb{V}$, the threshold of the number of inter-HAP links of a HAP, affects the quality of the cost estimation. To evaluate the choice of $\mathbb{V}$, we compared it with the number of inter-HAP links that a HAP finally has. Figure 14 shows the average number of inter-HAP links per HAP. When there were 40 wavelengths per link, the average number of inter-HAP links per HAP varied between 5.7 and 9.3 for $\mathbb{E}^{solar} \geq 50$ kWh and $\mathbb{V} = 10$, and between 8.8 and 11.8 for $\mathbb{E}^{solar} = 42$ kWh while $\mathbb{V}$ raised up to 12. Hence, the value of $\mathbb{V}$ was close to the actual number of inter-HAP links required by a HAP. However, when there were 80 wavelengths per link, the average number of Inter-HAP links per HAP was reduced to between 4.4 and 8.4, which is slightly far from the threshold $\mathbb{V} = 10$. A smaller $\mathbb{V}$ may help better estimate of the optimal cost in these cases.

VIII. CONCLUSION

Using *m*FSO configuration widens a HAP footprint, however, its application is constrained by the available solar energy of the HAP. Moreover, *m*FSO configuration may imply an extra investment cost due to additional *serving* FSO transceivers in comparison with single FSO transceiver configuration. This study focused on determining the optimal *m*FSO configuration. First, we proposed a set of closed-form expressions for computing the coverage of an *m*FSO configuration in terms of beam widths of the principal and supplementary transceivers and number of supplementary FSO transceivers. Second, we proposed an algorithm to determine the optimal *m*FSO configuration that minimizes the total HAP network cost. Third, we designed a HAP network topology using the optimal configuration to achieve a minimal final cost.

The simulation results showed that *m*FSO significantly extended the HAP footprint. With the testing dataset, the extended footprint radii were generally two times larger than the single FSO transceiver footprint radii, leading to a four-fold larger coverage surface. The network cost with the optimal *m*FSO configuration was as low as 54% of the network cost when using a single *serving* FSO transceiver on a HAP.

In the current study, all HAPs use identical *m*FSO configuration regardless the distribution of the ground nodes under it. The HAP network may be further optimized if each HAP adopt an individual *m*FSO configuration depending on communication demands from ground nodes under it.

.

APPENDIX A PROOF OF LEMMA 1

Proof: Let $x = \cos(\alpha/2)$, $a = \sigma\mathbb{H}$, and $b = \frac{P_{tx}\mathbb{R}_{rx}^2}{2\mathbb{H}^2}$ then

$$P_j^{rx}(x) = e^{-a/x}\frac{bx^2}{(1-x)} \tag{28}$$

Calculate the derivative of $P_j^{rx}(x)$ we get

$$P_j^{'rx}(x) = e^{-a/x}\left[\frac{a}{1-x} + \frac{2x-x^2}{(1-x)^2}\right]b \tag{29}$$

Thus, the derivative of $P_j^{rx}(\alpha)$ is

$$P_j^{'rx}(\alpha) = P_j^{'rx}(x) \times (-\sin(\alpha)) \tag{30}$$

Beam α is limited between $[0..\pi]$ because it orients to the ground. Thus, $x \in [0..1]$. Consequently, $1-x > 0$ and $2x - x^2 > 0$. In addition, $a, b > 0$, then $P_j^{'rx}(x) > 0$ for all $x \in [0..1]$. Because $-\sin(\alpha) < 0, \forall\alpha \in [0..\pi]$, thus, $P_j^{'rx}(\alpha) < 0$. Consequently, $P_j^{rx}(\alpha)$ decreases with α. ■

APPENDIX B CALCULATION OF EXTENDED COVERAGE RADIUS OF *m*FSO CONFIGURATION

This section identifies formulas that calculate the extended coverage radius of an *m*FSO configuration characterized by the principal beam width α, supplementary beam width β and number of supplementary beams m.

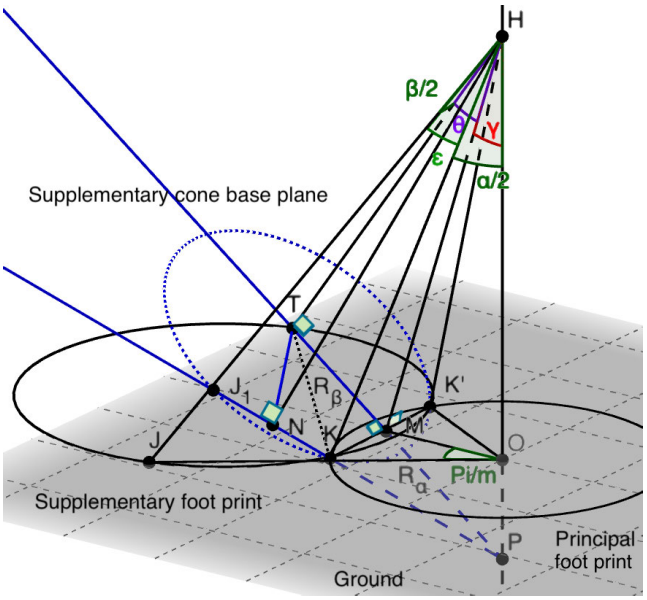

FIGURE 15. Computation of the distance from supplementary FSO transceivers and the border of extended coverage area L_J in function of Beta.

Conventionally, the coverage provided by a bundle of transmitters is calculated as if the transmitters project perpendicular to the ground. In *m*FSO configuration, the principal beam in the center is large, and it pushes the supplementary *serving* FSO transceiver projection directions far from perpendicular to the ground. These supplementary beams form oblique cones that intersect with the ground plane in ellipses. Considering of the elliptical form adds more complexity to the calculation.

In Figure 15, H denotes the position of a HAP, and its projection on the ground plane is O, thus $HO = \mathbb{H}$. The principal beam forms a right circular cone whose axis is HO. The cone intersects the ground plane by a circle of radius R_α, which defines the principal footprint. The beam of a supplementary FSO transceiver is an oblique cone intersecting the ground plane by an ellipse that defines the corresponding supplementary footprint. The cone of the supplementary beam intersects with the cone of the principal beam by two lines: HK and HK' where K and K' are the two intersection points of the principal and supplementary footprints. Thus, $OK = OK' = R_\alpha$.

m supplementary FSO transceivers are arranged evenly around the principal transceiver, each of which is responsible for extending the coverage within an angle of $2\pi/m$ from the center O. The responsible angle of the supplementary FSO transceiver in Figure 15 is defined by rays $\overrightarrow{OK}$ and $\overrightarrow{OK'}$. Thus, $\widehat{KOK'} = 2\pi/m$.

Ray $\overrightarrow{OK}$ intersects with the supplementary beam cone at J, then OJ is the radius of the extended coverage region. Readers refer to Figure 6 for a complete view of the extended coverage circle and the positions of K, K' and J on the ground.

Since the principal beam width is α, then $\widehat{OHK} = \alpha/2$.

Let the base plane containing K and K' of the supplementary beam cone cuts the cone axis at T, the primary cone axis HO at P, and HJ at J_1. Then $\widehat{THK} = \beta/2$. In addition, the supplementary cone intersects with this base plane by a circle containing K, K' with center T. Let R_β be the radius of the circle, then $TK = TK' = R_\beta$.

Let M be the midpoint of KK' then H, O, T, M belong to the same plane.

Let $\xi = \widehat{KHJ}$. The extended coverage radius is $R_{\text{ext}} = OJ = HO\tan(\widehat{OHJ}) = \mathbb{H}\tan(\frac{\alpha}{2} + \xi)$. Thus,

$$R_{\text{ext}} = \mathbb{H}\tan\left(2(\frac{\xi+\alpha}{2}) - \frac{\alpha}{2}\right)$$

$$\boxed{R_{\text{ext}} = \mathbb{H}\frac{2\tan(\frac{\xi+\alpha}{2}) - \tan(\frac{\alpha}{2})(1-\tan^2(\frac{\xi+\alpha}{2}))}{1-\tan^2(\frac{\xi+\alpha}{2}) + 2\tan(\frac{\xi+\alpha}{2})\tan(\frac{\alpha}{2})}} \quad (31)$$

A. CALCULATION of $\tan(\frac{\xi+\alpha}{2})$

Let N be the midpoint of KJ_1. As K and J_1 are at the intersection of the supplementary cone and its base plane, $HK = HJ_1$, $HN \perp KJ_1$, and HN is the angle bisector of $\widehat{KHJ_1}$. Therefore, $\widehat{NHK} = \xi/2$, thus $\widehat{NHP} = \frac{\xi+\alpha}{2}$. In addition, since KO is on the base plane of the principal cone, $HO \perp KO$. Thus, $\triangle PNH$ and $\triangle POK$ are similar right triangles. Consequently, $\widehat{OKP} = \widehat{NHP} = \frac{\xi+\alpha}{2}$. Furthermore,

$$\tan\left(\frac{\xi+\alpha}{2}\right) = \frac{OP}{OK} = \frac{OP}{R_\alpha} \quad (32)$$

Let $\widehat{OHM} = \gamma$ and $\widehat{THM} = \theta$ Then $\widehat{OHT} = \theta + \gamma$.

Because MO is on the base plan of the principal cone, $MO \perp HO$. In addition, as PT is on the base plane of the supplementary cone whose axis is HT then $HT \perp PT$. Consequently, $\triangle PTH$ and $\triangle POM$ are similar right triangles. We can deduce that $\widehat{PMO} = \widehat{PHT} = \theta + \gamma$. Therefore,

$$\tan(\theta+\gamma) = \frac{OP}{OM} = \frac{OP}{R_\alpha\cos(\frac{\pi}{m})}$$

Combining with eq. 32 we deduce:

$$\tan\left(\frac{\xi+\alpha}{2}\right) = \tan(\theta+\gamma)\cos\left(\frac{\pi}{m}\right) \quad (33)$$

Thus

$$\boxed{\tan\left(\frac{\xi+\alpha}{2}\right) = \frac{\tan(\gamma)+\tan(\theta)}{1-\tan(\gamma)\tan(\theta)}\cos\left(\frac{\pi}{m}\right)} \quad (34)$$

Since $\gamma = \widehat{OHM}$ then, $\tan(\gamma) = \frac{MO}{HO}$.
From right triangle $\triangle OMK$ we have $MO = OK\cos(\frac{\pi}{m})$.
From right triangle $\triangle HOK$ we have $HO = OK/\tan(\frac{\alpha}{2})$.
Thus

$$\boxed{\tan(\gamma) = \tan\left(\frac{\alpha}{2}\right)\cos(\pi m)} \quad (35)$$

It remains to calculate $\tan(\theta)$.

B. CALCULATION OF $\tan(\theta)$

Look at the right triangle $\triangle HTM$, we can see that:

$$\tan(\theta) = \frac{TM}{TH} \quad (36)$$

Since K and K' are on a circle centered at T, and M is the midpoint of KK' then $\triangle TMK$ is a right triangle, then

$$TM = \sqrt{TK^2 - KM^2} = \sqrt{R_\beta^2 - R_\alpha^2\sin^2\left(\frac{\pi}{m}\right)} \quad (37)$$

Easy to find that $\triangle THK$ is another right triangle then

$$TH = \frac{TK}{\tan(\frac{\beta}{2})} = \frac{R_\beta}{\tan(\frac{\beta}{2})} \quad (38)$$

Replacing (37) and (38) in to (36) we get

$$\begin{aligned}\tan(\theta) &= \frac{\sqrt{R_\beta^2 - R_\alpha^2\sin^2(\frac{\pi}{m})}}{R_\beta/\tan(\frac{\beta}{2})} \\ &= \tan\left(\frac{\beta}{2}\right)\sqrt{1-\left(\frac{R_\alpha}{R_\beta}\right)^2\sin^2\left(\frac{\pi}{m}\right)}\end{aligned} \quad (39)$$

From right triangle $\triangle HTK$ we obtain $R_\beta = HK\sin(\frac{\beta}{2})$.
From right triangle $\triangle HOK$ we obtain $R_\alpha = HK\sin(\frac{\alpha}{2})$.
Replacing these values to (39), we obtain:

$$\boxed{\tan(\theta) = \frac{\sqrt{\sin^2(\frac{\beta}{2}) - \sin^2(\frac{\alpha}{2})\sin^2(\frac{\pi}{m})}}{\cos(\frac{\beta}{2})}} \quad (40)$$

Substituting the values of $\tan(\gamma)$ in (35) and $\tan(\theta)$ in (40) into (34), we obtain $\tan(\frac{\xi+\alpha}{2})$. Subsequently, replacing the obtained $\tan(\frac{\xi+\alpha}{2})$ to (31) we get R_{ext}.

REFERENCES

[1] fSONA. *SONABeam 2500-E+ Model Specifications*. Accessed: Jan. 2022. [Online]. Available: http://fsona.com
[2] A. S. Acampora and S. V. Krishnamurthy, "A broadband wireless access network based on mesh-connected free-space optical links," *IEEE Pers. Commun.*, vol. 6, no. 5, pp. 62–65, Oct. 1999.
[3] J. Zhang, "Proposal of free space optical mesh network architecture for broadband access," in *Proc. IEEE Int. Conf. Commun. (ICC)*, vol. 4, Apr. 2002, pp. 2142–2145.
[4] T. C. Tozer and D. Grace, "High-altitude platforms for wireless communications," *Electron. Commun. Eng. J.*, vol. 13, no. 3, pp. 127–137, Jun. 2001.
[5] S. Karapantazis and F. Pavlidou, "Broadband communications via high-altitude platforms: A survey," *IEEE Commun. Surveys Tuts.*, vol. 7, no. 1, pp. 2–31, 1st Quart., 2005.
[6] Thales Group. (2017). *What's Up With Stratobus*. Accessed: Jan. 2022. [Online]. Available: https://www.thalesgroup.com/en/worldwide/space/news/whats-stratobus
[7] B. Moision, B. Erkmen, E. Keyes, T. Belt, O. Bowen, D. Brinkley, P. Csonka, M. Eglington, A. Kazmierski, N. H. Kim, J. Moody, T. Tu, and W. Vermeer, "Demonstration of free-space optical communication for long-range data links between balloons on project loon," *Proc. SPIE*, vol. 10096, pp. 259–272, Feb. 2017.
[8] C. Chen et al., "High-speed optical links for UAV applications," *Proc. SPIE*, vol. 10096, pp. 316–324, Mar. 2017.
[9] D. L. Truong, X. V. Dang, and T. N. Dang, "Survivable free space optical mesh network using high-altitude platforms," *Opt. Switching Netw.*, vol. 47, Feb. 2023, Art. no. 100716.

[10] G. K. Kurt, M. G. Khoshkholgh, S. Alfattani, A. Ibrahim, T. S. J. Darwish, M. S. Alam, H. Yanikomeroglu, and A. Yongacoglu, "A vision and framework for the high altitude platform station (HAPS) networks of the future," *IEEE Commun. Surveys Tuts.*, vol. 23, no. 2, pp. 729–779, 2nd Quart., 2021.
[11] R. Miura and M. Oodo, "Wireless communications system using stratospheric platforms: R and D program on telecom and broadcasting system using high altitude platform stations," *J. Commun. Res. Lab.*, vol. 48, pp. 33–48, Dec. 2001.
[12] D. L. Truong and T. N. Dang, "Beam size optimization for high-altitude platforms to ground links in FSO communications," *REV J. Electron. Commun.*, vol. 13, nos. 1–2, Jan./Jun. 2023, doi: 10.21553/rev-jec.332.
[13] V. V. Mai and H. Kim, "Beam size optimization and adaptation for high-altitude airborne free-space optical communication systems," *IEEE Photon. J.*, vol. 11, no. 2, pp. 1–13, Apr. 2019.
[14] A. A. Farid and S. Hranilovic, "Outage capacity optimization for free-space optical links with pointing errors," *J. Lightw. Technol.*, vol. 25, no. 7, pp. 1702–1710, Jul. 2007.
[15] H. Kunimori, M. Toyoshima, and Y. Takayama, "Overview of optical ground station with 1.5 m diameter," *J. Nat. Inst. Inf. Commun. Technol.*, vol. 59, no. 1.2, pp. 043–052, Mar. 2012.
[16] S. C. Arum, D. Grace, P. D. Mitchell, M. D. Zakaria, and N. Morozs, "Energy management of solar-powered aircraft-based high altitude platform for wireless communications," *Electronics*, vol. 9, no. 1, p. 179, Jan. 2020.
[17] F. Fidler, M. Knapek, J. Horwath, and W. R. Leeb, "Optical communications for high-altitude platforms," *IEEE J. Sel. Topics Quantum Electron.*, vol. 16, no. 5, pp. 1058–1070, Sep./Oct. 2010.
[18] Airbus. (2018). *Zephir: Persistance and Flexibility*. Accessed: Jan. 2022. [Online]. Available: https://lf5422.com/wp-content/uploads/2018/08/0296_18_2_zephyr_datasheet_e_horizontal_a4.pdf
[19] BAE Systems. (2018). *Phasa-35*. Accessed: Jan. 2022. [Online]. Available: http://prismaticltd.co.uk/products/phasa-35/
[20] N. T. T. Nguyen, M. B. Vu, H. T. Le, V. V. Mai, and N. T. Dang, "HAP-based multi-hop FSO systems using all-optical relaying and coherent receiver," in *Proc. 6th NAFOSTED Conf. Inf. Comput. Sci. (NICS)*, Dec. 2019, pp. 119–124.

DIEU LINH TRUONG received the Ph.D. degree from the Department of Computer Science and Operations Research, University of Montreal, Canada, in 2007. She was a Visiting Scholar with The University of Aizu, Japan, in 2010, Oklahoma State University, USA, in 2012 and 2013, and the Grenoble Institute of Technology, France, in 2019. She is currently an Associate Professor with the Faculty of Computer Engineering, School of Information and Communication Technology, Hanoi University of Science and Technology, Vietnam. Her research interests include optical networks and survivable network routing and design problems.

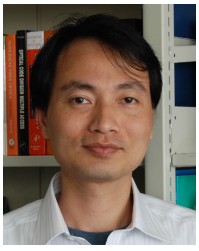

THE NGOC DANG (Member, IEEE) is currently an Associate Professor/the Vice Dean of the Faculty of Telecommunications and the Head of the Department of Wireless Communications, PTIT. He was also an invited Researcher with the FOTON ENSSAT Laboratory, Universite de Rennes 1, France, and a Research Fellow with the Computer Communications Laboratory, The University of Aizu. His current research interests include the areas of communication theory with a particular emphasis on modeling, design, performance evaluation of optical CDMA, RoF, QKD, and optical wireless communication systems.